Master-slave enhanced optical coherence microscopy for real-time optical biopsy imaging

Gianni Nteroli[a], Adrian Podoleanu[a], and Adrian Bradu[a*]

[a]Applied Optics Group, University of Kent, Canterbury, United Kingdom
* Corresponding author: a.bradu@kent.ac.uk

ABSTRACT

Diagnosing skin cancer, such as basal cell carcinoma, requires a biopsy, which is a time-consuming and expensive process. Therefore, it is essential to explore alternative diagnostic methods that are both more efficient and effective. We developed a handheld optical coherence microscopy (OCM) imaging device to achieve high-resolution optical biopsies in real-time. The instrument uses a variable focus liquid lens that allows fast shifting of the focus inside the sample, resulting in high-resolution lateral images throughout an extended axial imaging range. Our instrument can produce images with an axial resolution of approximately 5 μm, currently limited by the light source employed, and better than 2 μm transversal resolution images. The acquisition, data processing, and display of the 3D volumes are performed in real time, primarily enabled by the Master-Slave approach employed to produce the optical biopsies. The acquisition rate of the current camera used in the spectrometer was limited to 50 kHz. Our benchmarking shows that the real-time operation of the instrument can be sustained even at over 250 kHz solely by utilizing the computing power of the CPU, with no need to employ graphic cards or FPGAs. The instrument's capability is showcased through images featuring various samples, such as an IR card and skin.

Keywords: optical coherence tomography, optical biopsy, master-slave

1. INTRODUCTION

In clinical settings, noninvasive imaging techniques such as ultrasound, optical coherence tomography (OCT), and confocal microscopy are widely used to gain insights into the structural morphology of tissues. However, these methods often involve a spatial resolution and imaging depth tradeoff [1]. The imaging resolution and penetration depth determine the type of features that can be imaged, such as cellular and subcellular structures, and the depth at which they can be visualized within the tissue. A resolution better than 5 μm is desired to visualize cellular morphology, as typical cellular structures range from 10-20 μm. Moreover, an imaging depth of approximately 1 mm or more is advantageous for tracking cellular changes in tissue induced by various diseases [2].

Confocal microscopy provides a few microns or less lateral resolution, but its imaging depth is limited to tens of micrometers. Optical coherence tomography boasts remarkable imaging capabilities, with an axial resolution of just a few micrometers and a typical lateral resolution of tens of micrometers. One advantage of the OCT technology is that it decouples the transverse from the axial resolutions; another is that it can produce cross-sectional images in biological tissue exceeding 1 mm axially [3]. A trade-off between lateral resolution and axial range must be made when developing confocal microscopy and OCT instruments. Increasing NA improves resolution but reduces the depth of focus (DOF). An OCT imaging instrument equipped with a high NA objective (OCM instrument) can produce cellular imaging at the expense of a reduction in the DOF. To increase the axial imaging range, a technique utilizing the shifting of the focusing position inside the sample was introduced [4-6]. In this technique, the choice of wavelength range in the near-infrared was made, prioritizing lateral resolution over imaging depth and penetration into tissue. Multiple volumetric images of the sample are needed to obtain micron-resolution imaging over the entire volume. The number of volumes to be collected is equal to the ratio between the axial imaging range and the DOF, so if, for example, an axial imaging range of 1 mm is targeted and the DOF is 100 μm, 10 volumes must be acquired [7]. The production of the ten volumes, followed by joining them in real-time, is computationally expensive. The current spectral domain OCT technology in the near-infrared uses a linear camera. Therefore, the channeled spectra collected are inherently chirped and must be re-sampled [8]. The computation time of sequentially performing an interpolation of the channeled spectra and a Fast Fourier Transform is relatively time-

consuming [9]. In generating the final high-resolution volume, a massive amount of redundant data is produced (90% of the data produced is discarded when 10 volumes are generated).

The Master-Slave technique for generating OCT images can generate sub-volumes across axial ranges covering only the DOF; therefore, no redundant data is generated [10-12]. In this paper, we demonstrate a handheld instrument that can generate cellular-resolution images in real-time and, thus, can be used for applications where optical biopsies of non-stationary samples must be produced. We showcase the instrument's abilities by presenting several high-resolution images of various samples demonstrating exceptional lateral resolution.

2. THE EXPERIMENTAL SETUP

Figure 1 presents a schematic diagram of the handheld OCT imaging instrument we developed. Light from a superluminescent diode (SLD) with a central wavelength of 840 nm and a spectral bandwidth of 45 nm was employed. Light from the SLD is directed toward the sample via a 50/50 directional coupler DC. In the sample arm, light passes through two achromatic lenses (L1 and L2), a high numerical aperture microscope objective (MO, Olympus, LCPLN50XIR), and a variable focus liquid lens LL (diameter 5.8mm, NIR Coated, A-58N1-P20 Varioptic) which ensures fast shifting of the focus inside the sample. Two orthogonal galvo-scanners (GXY) scan the optical beam across the sample. The interference of light occurs at the DC between the light back-scattered by the sample and the light reflected by the mirror M placed in the reference arm of the interferometer. The channeled spectra are collected by using a spectrometer which includes two achromatic lenses (L5 and L6), a transmission diffraction grating (Wasatch Photonics, 1200 grooves per mm), and a linear camera (CAM, Basler, spL2048-70km). This camera can be run up to 70 kHz. However, the images presented in this paper are obtained with the camera operating at 50 kHz. Three electronic boards operating in synchronism were employed:

- an IMAQ board (National Instruments, PCIe-1429) was used to acquire the data;
- a multifunction I/O DAQ board (National Instruments, PCIe-1432) was used to generate waveforms to drive the galvo-scanners;
- a USB-M driver board was used to drive the liquid lens

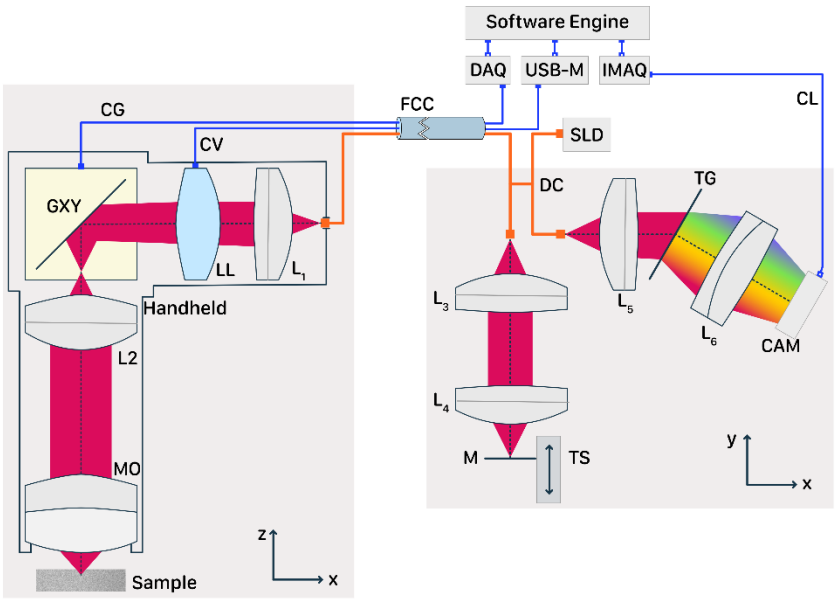

Figure 1. Schematic diagram of the instrument. L1-L6: achromatic lenses; MO: microscope objective; FCC: flexible cables conduit; CG and CV: electric cables connecting the galvos to the multi-function I/O DAQ and USB-M boards, respectively. CL: camera link cable; TG: transmission diffraction grating; GXY: pair of galvo-scanners; DC: directional coupler; SLD: superluminescent diode; CAM: linear camera.

An in-house LabVIEW software was developed to acquire data synchronously, drive the galvos and liquid lens, and generate real-time MS-based OCT images. The electric cables used to send driving voltages to the galvo-scanners and liquid lens, as well as the optical fiber conveying light toward the sample, were all inserted into a flexible cable conduit (FCC).

3. RESULTS

3.1 System characterization

The handheld OCT instrument was rigorously characterized. *En-face* OCT images of the USAF target were produced to evaluate the instrument's lateral resolution at various axial positions. Every time the axial position of the USAF target was changed, the liquid lens was driven to readjust the focus and regain the sharpness of the image. A typical image is presented in Fig. 2A. As one can observe, the smallest lines on the target (group 7, element 6) are separated; therefore, the lateral resolution that can be achieved is much better than 2.19 µm (the thickness of a single line) across an axial imaging range exceeding 1 mm. The DOF was measured by collecting the confocal signal (reference arm blocked) when, as a sample, a reflective mirror was used. We found that the value of the DOF is approximately 40 µm across the imaging range.

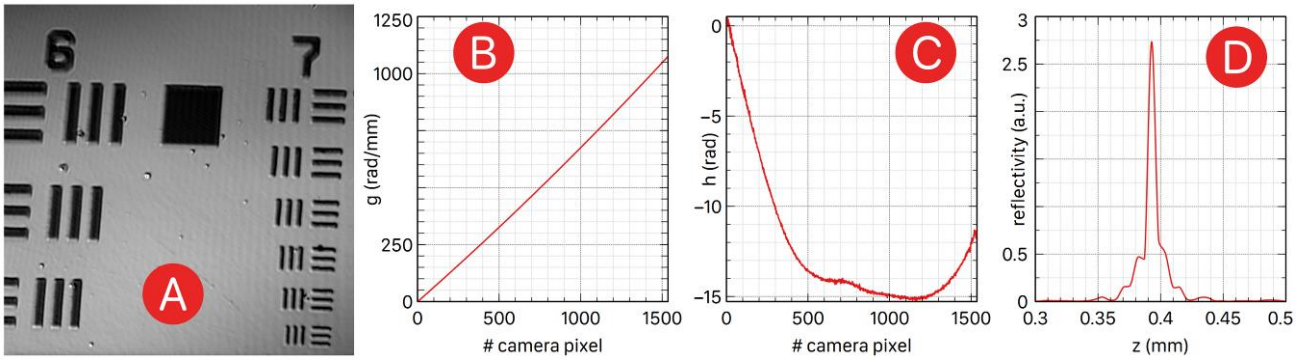

Figure 2. A. Experimental values of the energy per pulse (nJ) across imaging spectral range. B. Measurement of the lateral field of view of the instrument. The signal was collected while imaging a carbon fiber tape (along the dashed line shown in the inset image; the image size is 10×10 mm).

In Figs. 2B and 2C, the nonlinearity of the chirp of the channeled spectra across the camera's pixels (the g-function) and the unbalanced dispersion (the h-function) values across the camera's pixels are presented, respectively [8]. A typical A-scan obtained when imaging a highly reflecting object placed at about 0.4 mm from the position corresponding to the zero value of the optical path difference is presented in Fig. 2D. The full-width-at-half maximum of the peak obtained is used as an estimation of the axial resolution that the instrument can provide, which is approximately 5 µm. The sensitivity drop-off of the instrument is about 3 dB over an axial range of 1 mm). The position of the focus inside the sample does not change linearly with the voltage applied to the liquid lens. For this reason, a mapping of the voltages to be used to LL vs. the focusing position was experimentally determined before imaging.

3.2 Benchmarking

A triangular waveform was used to drive the position of the fast galvo-scanner. If the camera's acquisition rate is set to T_s and n_x is the number of A-scans contained in a B-scan, then the frequency at which the fast galvo-scanner is driven is $F_x=1/(2T_sn_x)$. This way, data is acquired for the first T_sn_x seconds, whereas the next T_sn_x seconds are used for data processing without the risk of losing any lines. Therefore, the instrument operates in real-time if the processing time is shorter than T_sn_x [9].

The linear camera used in the instrument has 2048 pixels. However, not all of them are used, as the spectrum was spread across 1536 pixels only. To investigate how the processing time depends on the number of pixels utilized, we have run the benchmarking for several n_k values (2048, 1536, and 1024 pixels). Our findings are summarized in Fig. 3, where the time needed to produce a B-scan image of size $n_x \times n_z$ is presented in different scenarios. In Fig. 3, data is shown for n_x=200. For benchmarking purposes, a dedicated LabVIEW software was run on a PC with a 12th-generation Intel Core i7-12700KF processor.

In Fig. 3, the blue lines show the time to produce a B-scan image using the FFT approach. In this case, when calculating the time needed to generate the image, we considered the time required to resample each of the 200 channeled spectra

using a cubic B-spline interpolation and the time to calculate their FFTs. The image size is $\mathbf{n_x \times n_k/2}$ when using the FFT technique. By zero padding, one can increase this number; however, the A-scan obtained will cover the same axial range as when no zero padding is performed. By decimation, the axial range can be reduced. However, it cannot be restricted to a specific axial region of interest. After performing the FFT operation, from the image obtained, only an area of interest of $\boldsymbol{n_x \times n_z}$ pixels is kept (the $\boldsymbol{n_z}$ pixels in the image must cover the length of the DOF). We did not consider the time to discard the redundant points outside the DOF in our benchmarking.

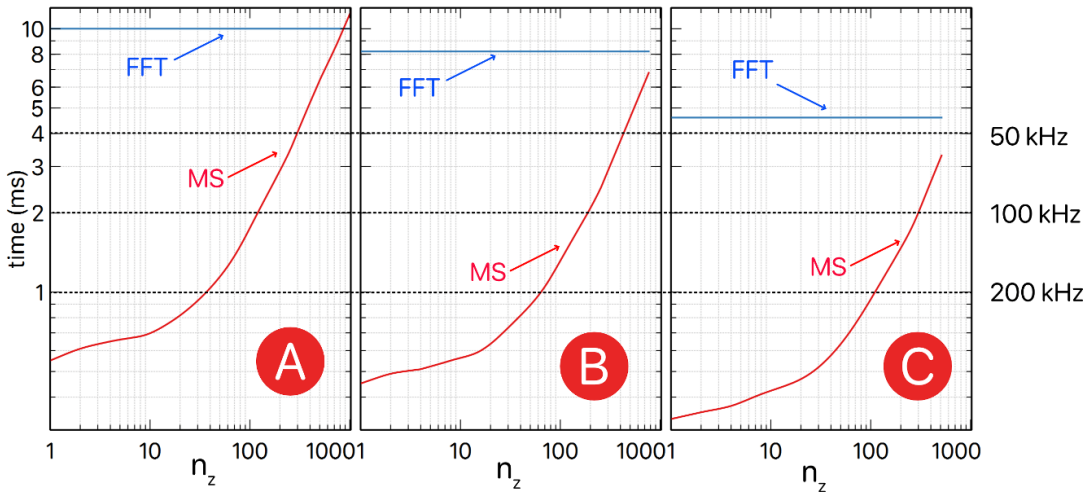

Figure 3. Vertical: the time of producing B-scan images containing 200 A-scans was determined using the FFT approach (blue curve) and MS (red curve). Horizontal: the number of axial pixels along depth. The FFT procedure always produces A-scans containing $n_k/2$ points. The number of points each channeled spectrum was digitized into is 2048 (A), 1536 (B), and 1024 (C). The dashed lines show the level up to which the instrument operates in real-time if the camera ran at 50 and hypothetically at 100 and 200 kHz, respectively.

The dashed lines in Fig. 3 show the time the data processing must be performed to ensure the real-time operation of the instrument. For example, when the camera works at 50 KHz, the real-time operation is achieved if the processing time is shorter than 4 ms. It is clear from Fig. 3 that if the FFT procedure is used, data is acquired faster than it is processed, and the instrument does not operate in real-time. If all 2048 pixels of the camera are used, the FFT processing time is around 10 ms; therefore, the only way for the instrument to operate in real-time is to slow down the acquisition rate to values below 20 kHz. Another option would be to reduce the number of sampling points (pixels) on the camera, which is not the ideal solution as this number of points $\boldsymbol{n_k}$ must drastically be reduced (as observed in Fig. 3C, the operation is not happening in real-time, not even for 1024 pixels).

In contrast to the FFT approach, the MS technique allows for real-time operation as the number of points in the A-scan can be adjusted to match the axial region of interest perfectly. If $\boldsymbol{n_k}$=2048 and the camera is operated at 50 kHz, the real-time operation is achieved for $\boldsymbol{n_z}$=300 or less axial points. As in our setup, the DOF is around 40 µm, and we consider an axial resolution of 5 µm; 16 axial points are needed only to produce a B-scan with an axial imaging depth equal to that of the DOF. When using the MS procedure, an image of size 200×16 can be generated in less than 1 ms, so in principle, the real-time operation is ensured for a faster acquisition rate than that of the camera our instrument is currently equipped with.

3.3 Images

In this sub-section, we present images captured by our state-of-the-art OCM instrument, which showcase valuable insights into the samples' structure and composition. These images are presented in Figs. 4, 5, and 6.

En-face OCT images of size 200×200 µm were obtained by imaging various samples, including paper, infrared cards, orange fruits, and biological samples, at depths ranging from 200 to 500 µm beneath the surface.

In Fig. 5, 16 consecutive OCT *en-face* images collected along the depth of focus were averaged to produce each of the six images; therefore, their axial resolution is 40 µm. Each of the images is made of 400×400 pixels. Consequently, they were collected in 6.4 s.

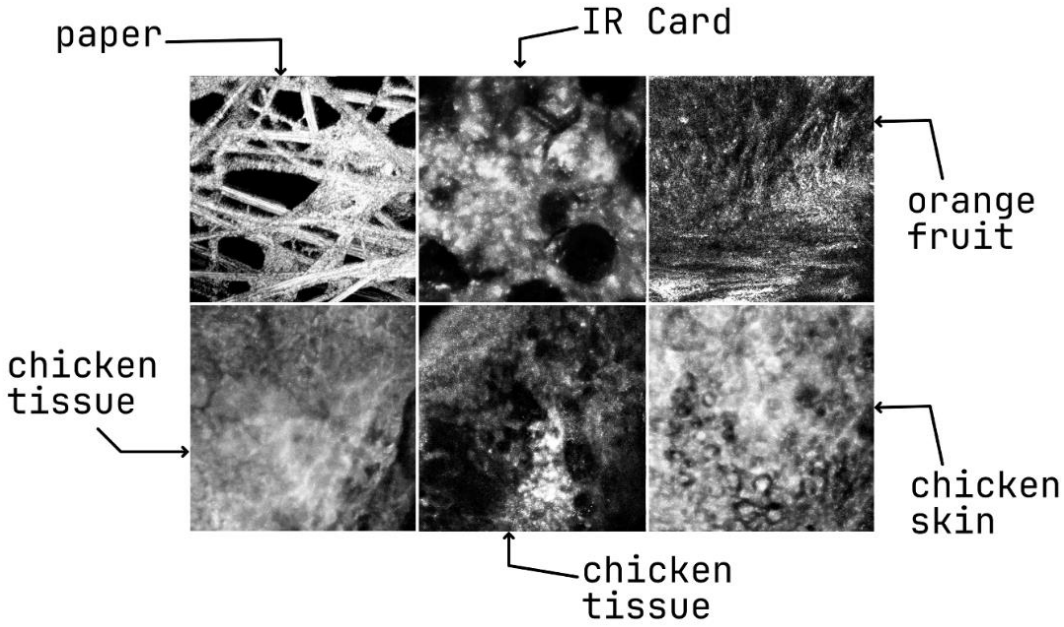

Figure 4. High-quality visuals showcase *en-face* images of tissue paper, IR card, orange fruit, and chicken tissue. Each image is approximately 200×200 µm.

Fig. 5 displays 12 *en-face* images acquired from axial positions 20 µm apart, covering a total axial range of 240 µm. The images were generated by moving the focus six times, and the entire process took 38.4 seconds.

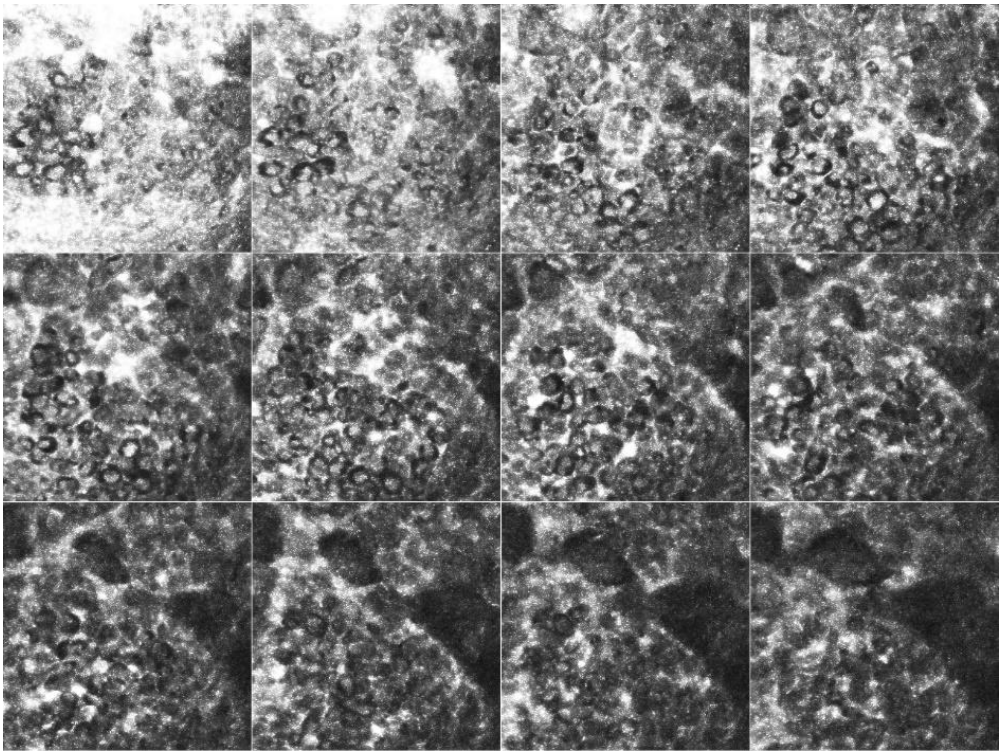

Figure 5. High-quality images that showcase 12 *en-face* OCT images of chicken skin tissue separated by 20 µm. Each image is approximately 200×200 µm.

Figure 6 illustrates the instrument's capability to produce images from different depths. It uses "hyper-spectral" *en-face* OCT technology, which assigns different colors to differentiate between images captured from various depths. The images are displayed using a "spectrum" look-up table. The color-coded images in red are collected from deeper inside the sample. Each image has a depth extension of approximately 5 μm in tissue, and the number of images per sample varies depending on the object being imaged.

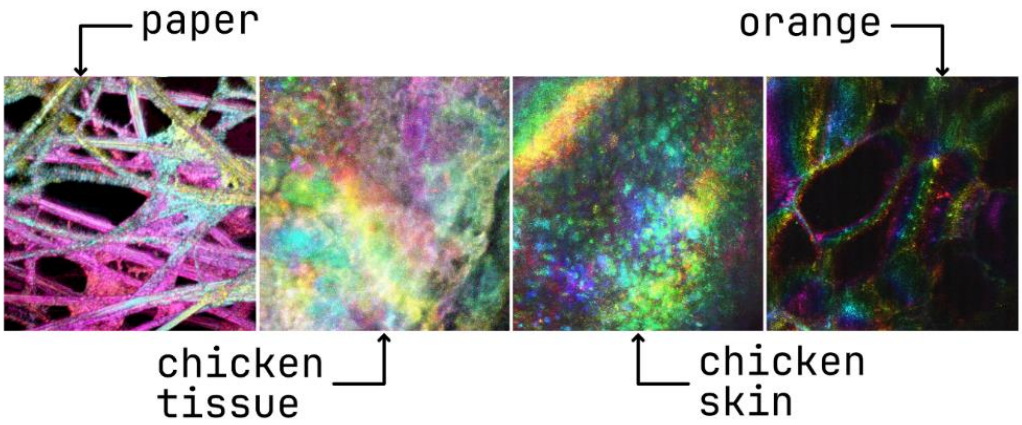

Figure 6: Hyperspectral *en-face* images collected from various axial positions. The spectrum lookup table is used to color code the axial position of each image. The separation between images is 5 um. The red-coded images are collected from a deeper axial position than the blue-coded ones.

4. CONCLUSIONS

This paper presents a handheld imaging device that can produce high-resolution lateral and axial resolution images. By shifting the focus inside the sample and carefully selecting the optical components embedded within the handheld, the lateral resolution is kept constant at less than 2 micrometers across an axial imaging range of around 1 millimeter. The experimentally measured axial resolution, determined by the characteristics of the optical source used, is 5 micrometers. The device is based on the Master-Slave procedure of generating images and is shown to produce images in real-time, without post-processing. The acquisition speed of the camera (50 kHz in our case) determines the time required to generate the combined volumes employed.

Our benchmarking indicates that images can still be produced in real-time at least five times faster if a faster acquisition speed camera is employed. We believe this device can revolutionize the diagnosis process by utilizing a non-invasive method that does not require tissue removal. While current OCT instruments cannot produce real-time optical biopsies equivalent to conventional ones, our portable instrument can produce high-definition images comparable to those obtained using traditional biopsies without requiring additional hardware resources and post-processing procedures.

5. ACKNOWLEDGMENTS

GM thanks the University of Kent for its support. AP and AB acknowledge the support of the Biological Sciences Research Council (BBSRC), “5DHiResE” project, BB/S016643/1; AP also acknowledges the European Union’s Horizon 2020 research and innovation program under the Marie Sklodowska-Curie grant NETLAS (agreement No 860807) and the NIHR Biomedical Research Centre BRC3 and NIHR BRC4-05-RB413-302, Imaging, Visual Assessment & Digital Innovation, at Moorfields Eye Hospital NHS FT and UCL Institute of Ophthalmology, University College London (AP). AB acknowledges the support of the Royal Society, project PARSOCT, RGS/R1/221324, and support of the Academy of Medical Sciences/the Wellcome Trust/the Government Department of Business, Energy and Industrial Strategy/the British Heart Foundation/Diabetes UK Springboard Award SBF007\100162.

REFERENCES

[1] Canavesi C, and Rolland J.P., "Ten Years of Gabor-Domain Optical Coherence Microscopy," Applied Sciences, **9** 2565 (2019).

[2] Leitgeb, R.A., "En-face optical coherence tomography: a technology review," Biomed. Opt. Express **10**, 2177-2201 (2019).

[3] Drexler, W., Liu, M., Kumar, A., Kamali, T., Unterhuber, A., Leitgeb, and R.A., "Optical coherence tomography today: speed, contrast, and multimodality," Journal of Biomedical Optics, **19**, 071412 (2014).

[4] Jannick P. Rolland, Panomsak Meemon, Supraja Murali, Ilhan Kaya, Nicolene Papp, Kevin P. Thompson, and Kye-Sung Lee "Gabor domain optical coherence microscopy", Proc. SPIE 7372, Optical Coherence Tomography and Coherence Techniques IV, 73721K (2009).

[5] Tankam P, He Z, Thuret G, Hindman HB, Canavesi C, Escudero JC, Lépine T, Gain P, Rolland JP. Capabilities of Gabor-domain optical coherence microscopy for the assessment of corneal disease. J Biomed Opt. 2019 Apr;24(4):1-17.

[6] Jannick P. Rolland, Panomsak Meemon, Supraja Murali, Kevin P. Thompson, and Kye-sung Lee, "Gabor-based fusion technique for Optical Coherence Microscopy," Opt. Express **18**, 3632-3642 (2010)

[7] Cernat, R., Bradu, A., Israelsen, N.M., Bang, O., Rivet, S., Keane, P.A., Heath, D., Rajendram, R., and Podoleanu, A., "Master/slave: a better tool for Gabor filtering optical coherence tomography imaging instruments," Proc SPIE, 104160N (2017).

[8] Bradu, A., Israelsen, N.M., Maria, M., Marques, M.J., Rivet, S., Feuchter, T., Bang, O., and Podoleanu, A., "Recovering distance information in spectral domain interferometry," Scientific Reports **8**, 15445 (2018).

[9] Bradu, A., Kapinchev, K., Barnes, F., and Podoleanu, A., "On the possibility of producing true real-time retinal cross-sectional images using a graphics processing unit enhanced master-slave optical coherence tomography system," J. Biomed. Opt., **20**, 076008 (2015).

[10] Bradu, A., Maria, M., and Podoleanu, A., "Demonstration of tolerance to dispersion of Master/Slave Interferometry," Opt. Express, **23** 14148-14161 (2015).

[11] Bradu, A., and Podoleanu, A., "Calibration-free B-scan images produced by master/slave optical coherence tomography," Opt. Lett. **39**, 450-453 (2014).

[12] Rivet, S., Maria, M, Bradu, A., Feuchter, T., Leick, L., and Podoleanu, A., "Complex master slave interferometry," Opt. Express **24**, 2885-2904 (2016).